JCTC Journal of Chemical Theory and Computation

Carbon−Hydrogen Bond Activation in Hydridotris(pyrazolyl)borate Platinum(IV) Complexes: Comparison of Density Functionals, Basis Sets, and Bonding Patterns

Benjamin Alan Vastine, Charles Edwin Webster,† and Michael B. Hall*

Department of Chemistry, Texas A&M University, P.O. Box 30012, College Station, Texas 77841-3012

Received May 18, 2007

Abstract: The reaction mechanism for the cycle beginning with the reductive elimination (RE) of methane from κ^3-TpPt^{IV}(CH$_3$)$_2$H (**1**) (Tp = hydridotris(pyrazolyl)borate) and subsequent oxidative addition (OA) of benzene to form finally κ^3-TpPt^{IV}(Ph)$_2$H (**19**) was investigated by density functional theory (DFT). Two mechanistic steps are of particular interest, namely the barrier to C−H coupling (barrier 1 − Ba1) and the barrier to methane release (barrier 2 − Ba2). For 31 density functionals, the calculated values for Ba1 and Ba2 were benchmarked against the experimentally reported values of 26 (Ba1) and 35 (Ba2) kcal·mol^{-1}, respectively. Specifically, the values for Ba1 and Ba2, calculated at the B3LYP/double-ζ plus polarization level of theory, are 24.6 and 34.3 kcal·mol^{-1}, respectively. Overall, the best performing functional was BPW91 where the mae associated with the calculated values of the two barriers is 0.68 kcal·mol^{-1}. The calculated B3LYP values of Ba1 ranged between 20 and 26 kcal·mol^{-1} for 12 effective core potential basis sets for platinum and 29 all-electron basis sets for the first row elements. Polarization functions for the first row elements were important for accurate values, but the addition of diffuse functions to non-hydrogen (+) and hydrogen atoms (++) had little effect on the calculated values. Basis set saturation was achieved with APNO basis sets utilized for first-row atoms. Bader's "Atoms in Molecules" was used to analyze the electron density of several complexes, and the electron density at the Pt−N$_{ax}$ bond critical point (trans to the active site for C−H coupling) varied over a wider range than any of the other Pt−N bonds.

Introduction

The goal of facile conversion of saturated hydrocarbons into desirable organic materials motivates C−H bond activation research, and platinum is an important metal for these reactions.[1] Garnett and Hodges[2] were the first to report platinum mediated C−H bond activation, and they observed H/D exchange between deuterated water and aromatic substrates catalyzed by Pt^{II} salts in an acidic solution. Shilov and co-workers[3] investigated the catalytic oxidation of methane to methanol and chloromethane by $PtCl_4^{2-}$ and $PtCl_6^{4-}$ salts in acidic aqueous solution. The research into mechanistic aspects related to the Shilov chemistry is chronicled in two reviews,[4] and they include a discussion of the formation of 5-coordinate, coordinatively unsaturated Pt^{IV} complexes and their purported role in the reductive elimination (RE) step.

The isolation of 5-coordinate Pt^{IV} complexes is important because they are believed to be intermediates in platinum-mediated oxidative addition (OA) and RE chemistry. The first isolated 5-coordinate Pt^{IV} alkyl complex[5] was implicated in C−C bond-forming RE chemistry,[6] and Goldberg and co-workers[7,8] proposed 5-coordinate, coordinatively-unsaturated

* Corresponding author e-mail: hall@science.tamu.edu.

† Present address: Department of Chemistry, The University of Memphis, 213 Smith Chemistry Building, Memphis, TN 38152-3550.

10.1021/ct700120d CCC: $37.00
Published on Web 09/14/2007

Scheme 1

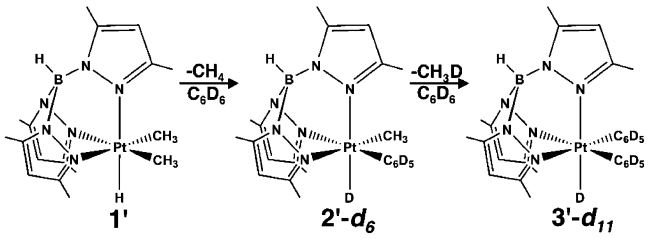

Pt^{IV} complexes as intermediates in C−H and C−C RE coupling reactions. Templeton and co-workers[9] isolated three different 5-coordinate Pt^{IV} complexes that were stabilized by silanes and proposed several 5-coordinate Pt^{IV} complexes as intermediates.[10,11]

In a theoretical study of Shilov chemistry, Siegbahn and Crabtree[12] argued that a σ-bond metathesis mechanism is preferred over the OA/RE mechanism; however, the possibility of the oxidative pathway could not be eliminated because of the similar energetics to that of metathesis. They also stated that the solvent was integral to the reaction. Bartlett et al. reported two studies of RE C−H coupling that used Pt^{II} and Pt^{IV} model complexes,[13] and both reports arrived at the same conclusion. For Pt^{II} complexes, direct elimination of methane was found to be favored energetically over phosphine loss prior to RE C−H coupling, but ligand loss prior to C−H coupling was preferred for the Pt^{IV} complexes.

Jensen et al.[14] reported the RE of methane and OA of benzene-d_6 to form κ^3-$Tp^{3,5-Me}Pt^{IV}(C_6D_5)_2D$ from κ^3-$Tp^{3,5-Me}$-$Pt^{IV}(CH_3)_2H$ (**1′**), where $Tp^{3,5-Me}$ (or Tp*) is the hydridotris-(3,5-dimethylpyrazolyl)borate ligand (Scheme 1).[15] From the kinetic studies, enthalpic barriers to methane formation (barrier 1 − Ba1) and methane release (barrier 2 − Ba2) from **1′** were measured and reported. The proposed mechanistic step for Ba1 is C−H coupling between a methyl ligand and the hydride of **1′**, and for Ba2, methane elimination from **1′**. The authors concluded that this elimination precedes benzene addition, which is consistent with a dissociative mechanism. Another recent report also concluded that the dissociative mechanism is the preferred pathway for methane elimination from Pt^{IV} complexes.[16] Suggestions have been made that the Tp* ring trans to the hydride could dechelate, bind in a κ^2-interaction to the platinum center, and provide an open coordination site. Zarić and Hall reported that loss of one degree of coordination of the Tp ligand ($\kappa^3 \rightarrow \kappa^2$) occurred prior to methane activation in a TpRh(CO) complex.[17]

Here, the results of a density functional theory[18] (DFT) study on the reaction in Scheme 1 are presented. Specifically, 31 density functionals and a variety of basis sets are benchmarked against the experimental values of Ba1 and Ba2 that were reported by Jensen et al.[14] For some of the reported results, the experimental Tp* ligand (**1′**, etc.) is replaced with the parent Tp ligand (**1**, etc.). The basic mechanism for the reaction studied is presented in section 1, and possible alternative pathways for the mechanism of C−H coupling and methane release are examined in section 2. The bonding schemes of several complexes are presented in section 3; studies in benchmarking DFT and various basis sets against the experimental values for Ba1 and Ba2 are presented in section 4.

Results and Discussion

1. Mechanism. In the following section, specific steps of the mechanism from the dimethyl reactant (**1**) to the methyl-phenyl intermediate (**10**) are studied. The mechanism and relative energies of the two barriers and the specific coordination modes of benzene in the methyl−benzene complexes (**6** and **8**) are presented and discussed. Then, the analogous reaction pathway for the release of the second methane and coordination of the second benzene to form the final diphenyl product (**19**) is presented.

Procedure. All calculations were performed by using the Gaussian 03 suite of programs.[19] Each complex reported in this section was fully optimized at the B3LYP/BS1 level of theory, and the analytical frequencies were calculated at this same level of theory for each complex to determine if the force constants were real (intermediate) or if one was imaginary (transition state). All optimizations were accomplished with the default convergence criteria, and each complex was optimized in C_1 symmetry. The B3LYP hybrid density functional is comprised of the Becke3 exchange functional and the Lee, Yang, and Parr correlation functional.[20] The basis set (BS1) that was used in the optimization and frequency calculations is as follows: platinum was assigned the Hay and Wadt small core Los Alamos National Laboratory effective core potential[21] (ECP = LANL2) and the valence double-ζ (341/341/21 = DZ) basis set (BS) as modified by Couty and Hall (ECP/BS = mLANL2DZ);[22] each nitrogen, boron, and the carbon and hydrogen atoms bound to the platinum were assigned Dunning's correlated consistent polarized valence double-ζ (cc-pVDZ) basis set;[23] all other atoms were assigned Dunning's full double-ζ D95 basis set.[24] Details for the density functionals and basis sets benchmarking studies will be given later. Unless noted otherwise, all energies are in kcal·mol^{-1} and relative to **1**. Most values discussed in the text are enthalpies ($\Delta H^{\circ/\ddagger}$) in the gas phase at standard conditions (298 K, 1 atm). The electronic energies (ΔE_{elec}), electronic energies with zero point corrections (ΔE_0), and free energies ($\Delta G^{\circ/\ddagger}$) are reported in tables. Three-dimensional molecular geometric representations were constructed with JIMP 2.[25]

κ^3-$TpPt^{IV}(CH_3)_2H$ (1) + C_6H_6 to κ^3-$TpPt^{IV}(CH_3)$-$(C_6H_5)H$ (10) + CH_4. The B3LYP/BS1 reaction energy profile for reductive elimination (C−H bond formation), methane release, benzene coordination, and oxidative addition of benzene is displayed in Figure 1. The orientations of the ligand atom positions in the complexes, as referenced in the text, are defined in Figure 2. The relative energy values (**1** + benzene = 0) for species **1**−**10** are tabulated in Table 1. The B3LYP/BS1 optimized geometries of complexes along the potential energy surface (PES), with relevant bond distances (Å), are shown in Figure 3.

C−H Coupling through Reductive Elimination of Methane (Ba1). In reactant **1**, the stronger trans influence of the hydride is noticeable in the slightly longer $Pt-N_{ax}$ bond. The transition state for the C−H coupling mode (**2-TS**) has an enthalpic barrier of 24.3 kcal·mol^{-1} and can be

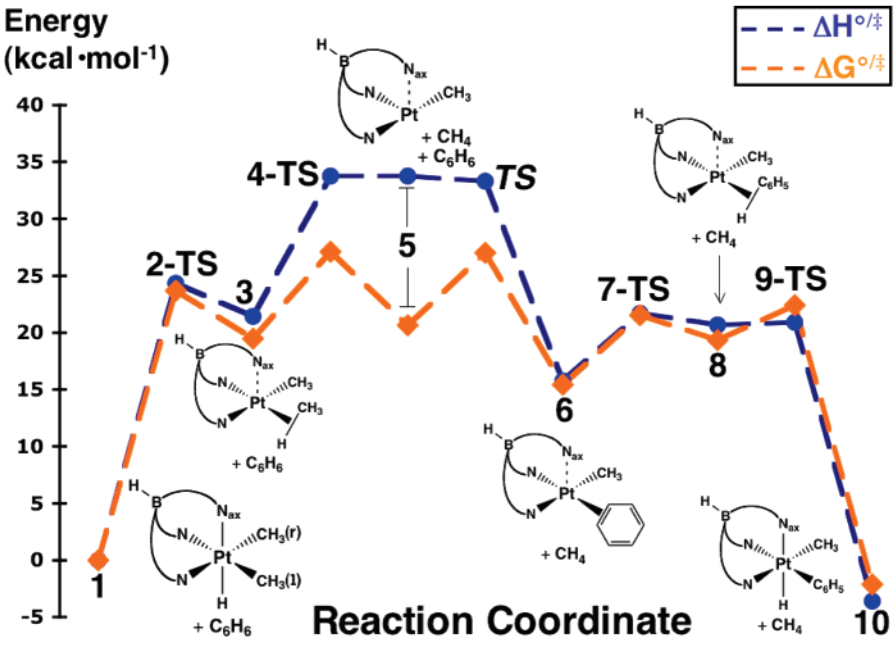

Figure 1. The B3LYP/BS1 relative enthalpies (blue) and free energies (orange) for complexes **1**−**10** (kcal·mol^{-1}). The complex designations correspond to the structures listed in Figure 3 and Table 1. The TS that connects **5** and **6** (***TS***) *was not calculated* and is only a qualitative representation.

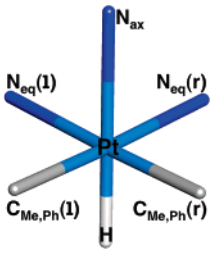

Figure 2. A generalized model that illustrates the orientations of the atoms within the ligands. These assignments are referenced in the text.

Table 1. Relative B3LYP/BS1 Energies for Complexes **1**−**10**

	energies			
complex	ΔE_{elec}	ΔE_0	$\Delta H^{\circ/\ddagger}$	$\Delta G^{\circ/\ddagger}$
1[a]	0	0	0	0
2-TS[a]	24.15	24.14	24.33	23.70
3[a]	20.82	20.82	21.43	19.49
4-TS[a]	32.28	32.28	33.76	26.90
5[a,b]	32.56	32.56	33.76	20.64
6[b]	14.46	14.46	15.76	15.42
7-TS[b]	20.58	20.58	21.68	21.52
8[b]	19.20	19.20	20.67	19.33
9-TS[b]	20.06	20.06	20.92	22.40
10[b]	−4.55	−4.55	−3.60	−2.15

[a] + C_6H_6. [b] + CH_4 energy values are given in kcal·mol^{-1} and are relative to **1**.

characterized as a late transition state in which the C_{Me}(l)−Pt−H angle has decreased by more than half its original value. This transition state leads to the formation of the relatively unstable intermediate **3** where the Pt−C_{Me}(l) bond has lengthened by 0.35 Å, and the C−H bond is 1.17 Å. During this process the Pt−N_{ax} progressively lengthens, and **3** is essentially a 4-coordinate square planar complex as expected for a d^8 metal (Pt^{II}). The Pt−N_{eq}(r), which is trans to the weakly bound CH_4 molecule, has shortened by 0.2 Å.

Methane Loss from 3 (Ba2). When the weakly bound CH_4 ligand of **3** is released, the Pt−N_{eq}(r) bond shortens to its minimum length (1.98 Å). The unimolecular dissociation transition state (**4-TS**) for this process is characterized by an enthalpic difference of 33.8 kcal·mol^{-1} (relative to **1**) and results in a coordinatively unsaturated (3-coordinate), 16e$^-$ Pt^{II} (d^8) species (**5**) where the Pt−N_{ax} distance shortens slightly from that of **3**. This intermediate, **5**, is nearly isoenthalpic with **4-TS**, and this result is explained below. The Pt−C_{Me}(r) and −N_{eq}(l) bond lengths are unaffected by methane release.

Common assumptions for the dissociation of a neutral dative ligand from a transition-metal complex that does not rearrange following a dissociation are as follows: (1) that entropy does not contribute until after the transition state is passed and (2) no enthalpic barrier exists for the recoordination.[26] With this assumption the free energy barrier ($\Delta G^{\ddagger}$) equals the enthalpic barrier ($\Delta H^{\ddagger}$). In Figure 4, the relative enthalpies and free energies versus length of the Pt−C_{Me}(l) coordinate starting from **3** are plotted for six points; the enthalpy curve plateaus at 4.42 Å and a value of 34 kcal·mol^{-1}, while the free energy curve plateaus at a length of 3.62 Å and a value of 26 kcal·mol^{-1}. The dissociation transition state, **4-TS**, is chosen to be located at 4.42 Å because both curves have plateaued by this point, and **4-TS** is isenthalpic with the relative enthalpy difference between **1** and **5**. Our primary purpose here is to consider the enthalpic barrier to methane release, and we have shown that the enthalpic difference between the separated products and the starting material is a good approximation for the experimental enthalpic barrier; therefore, *Ba2 is defined as the calculated relative enthalpic difference between **1** and **5** (+free methane)*. The relative free energy difference does not

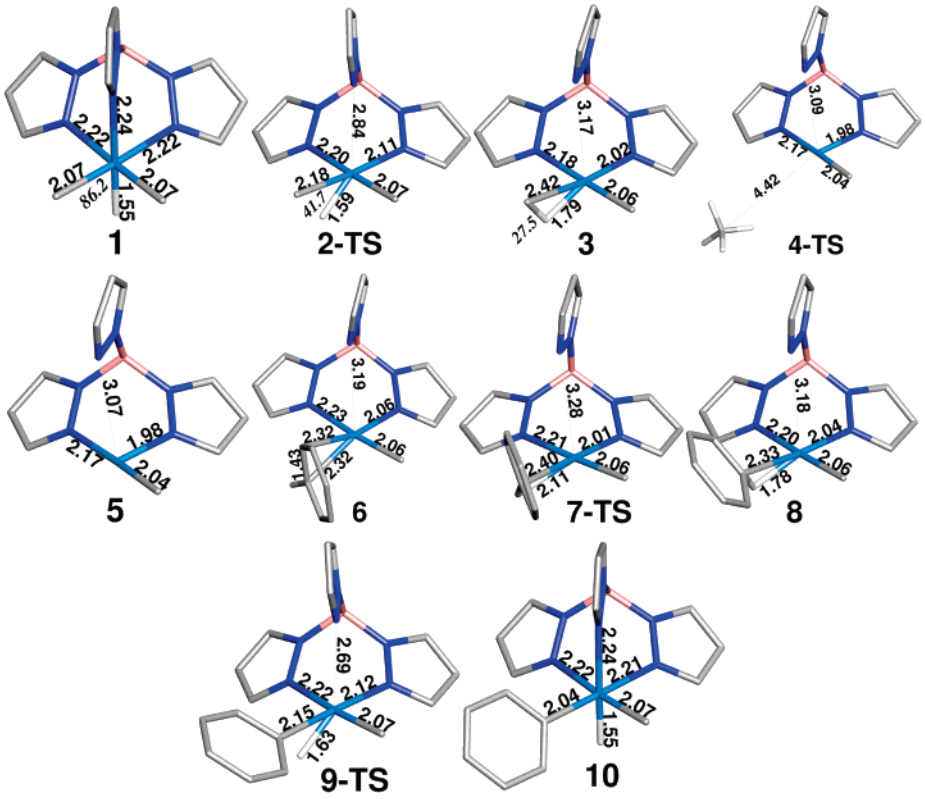

Figure 3. The optimized geometries for complexes **1**−**10**. Relevant bond lengths are included in the representations and are given in Å. The C_{Me}(l)−Pt−H angles (deg) are the numbers in italics. All nonessential hydrogen atoms have been removed for clarity.

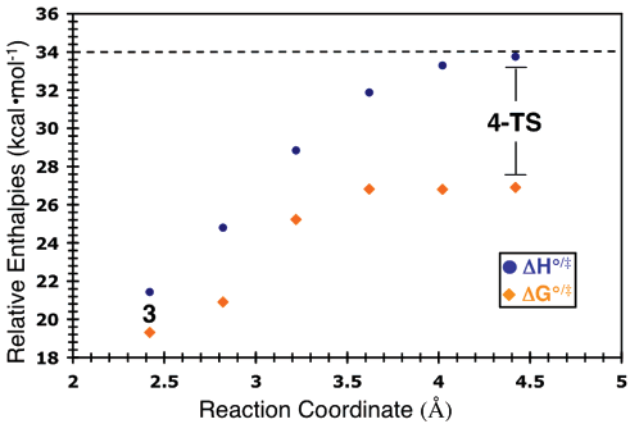

Figure 4. Relative enthalpy and free energy values for six select points along the Pt−$C_{\sigma-Me}$(l) coordinate. The dashed line represents the calculated enthalpic value for Ba2 (**4-TS**).

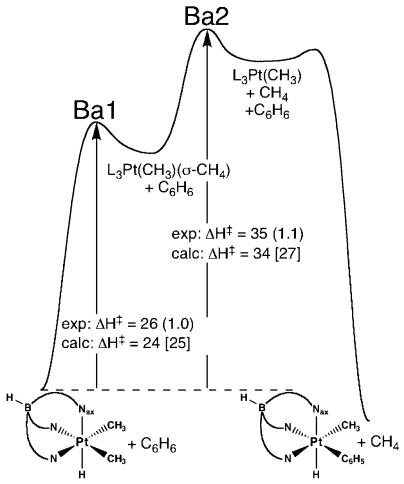

Figure 5. Comparison of the experimental and B3LYP/BS1 values for Ba1 and Ba2 (kcal·mol^{-1}). The Tp and Tp* ligands are denoted as "L_3". The reported uncertainties are given in parenthesis after the experimental values. The values in square brackets are the calculated values relative to **1′**.

increase at the same rate as the enthalpy, so there is a contribution of the entropy to the transition state. The difference between the common assumption and the free energy difference calculated for **4-TS** is 4.9 kcal·mol^{-1}, ca. 38% of the total entropy for the dissociation to **5** (+free methane).

Barriers 1 and 2. The experimental and calculated barriers (Ba1 and Ba2) are compared in Figure 5 where the energies are reported for Tp (**1** = 0.0) and for Tp* (**1′** = 0.0) in square brackets, and we observe agreement within two units of experimental uncertainty between the calculated and experimental value for both barriers; however, both calculated values are slightly less than the experimental value. For methane release from **1′**, the B3LYP/BS1 value for Ba1 is similar to that of **1**; however, the value for Ba2 is 8 kcal·mol^{-1} less than experiment. The Pt−N_{ax} distance of **5′** (2.15 Å) is 0.92 Å shorter than that of **5** (3.07 Å), and the

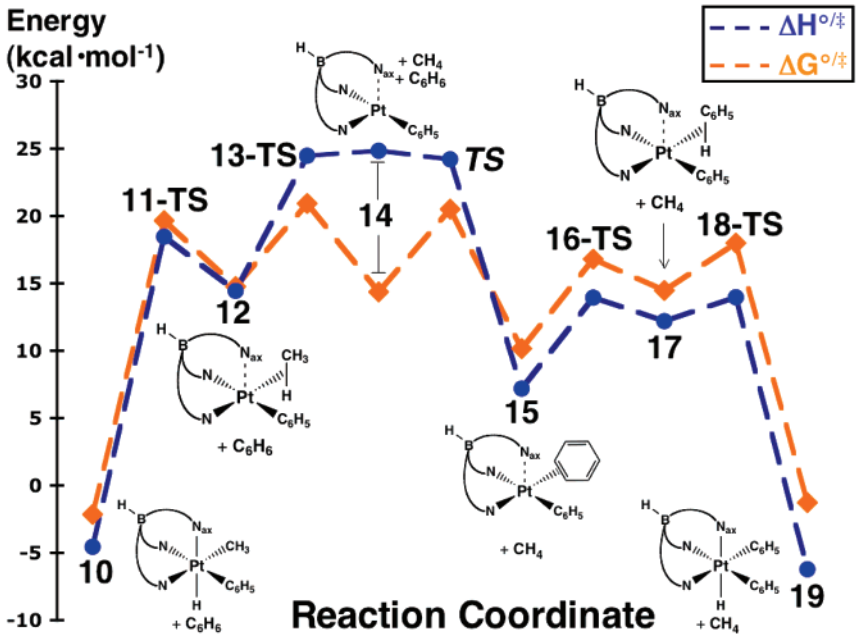

Figure 6. The B3LYP/BS1 calculated relative enthalpies (blue) and free energies (orange) in kcal·mol^{-1} for **10**−**19** (values relative to **1**). The species included in the figure are representative of those listed in Supporting Information Figure 1 and Table 2. The TS that connects **14** and **15** (***TS***) *was not calculated* and is only a qualitative representation.

result is the stabilization of the coordinatively unsaturated intermediate.

Benzene Coordination and OA To Form κ^3-TpPt^{IV}-(CH$_3$)(C$_6$H$_5$)H (10). The transition state for benzene coordinating to **5** (***TS*** − Figure 1) was not located on the B3LYP/BS1 PES, and its value was assumed to be similar to **4-TS**. There are two coordination modes for benzene to **5** that are in agreement with experimental observations:[27] (1) an η^2-benzene bound through two carbons (π bond) forming complex **6** and (2) a σ-bound complex forming an η^2-benzene bound through a C−H bond (**8**). Species **6** is more stable than **8** by 4.91 kcal·mol^{-1}, and they are connected through **7-TS** with a barrier of 5.92 kcal·mol^{-1} (relative to **6**). Benzene acts as a π-donor/acceptor in **6** as the calculated carbon−carbon bond length of the two carbons π-bound to the platinum center (1.43 Å) is slightly longer than that calculated for the carbon−carbon bond length of free benzene (1.40 Å). The Pt−N$_{eq}$(r) bond length is slightly longer in **6**, which, coupled with the relative enthalpy difference, supports the view that benzene is in the π-bound form. Reinartz et al. reported[10] geometric parameters of an isolated η^2 benzene complex that is analogous to **6**, and the calculated parameters of **6** agree well with their complex; the experimentally determined Pt−C, Pt−N$_{eq}$(r), and C−C bond lengths are shorter compared to those in **6** by 0.08, 0.07, and 0.02 Å, respectively. The geometries of **6** and **8** are pseudo square planar (4-coordinate) at platinum, and the Pt−N$_{ax}$ distance is long for both. The facile OA splitting of the σ-C−H bond occurs (**9-TS**) to form the pseudo-octahedral complex, **10**. Overall, the exchange of phenyl for methyl is slightly exothermic.

From κ^3-TpPt^{IV}(CH$_3$)(C$_6$H$_5$)H (10) to κ^3-TpPt^{IV}(C$_6$H$_5$)$_2$H (19). The B3LYP/BS1 reaction profile for the elimination of the second methane and addition of the second benzene (**10**−**19**) is shown in Figure 6 and is analogous to Figure 1.

Table 2. Relative B3LYP/BS1 Energies for Complexes **10**−**19**

	energies			
complex	ΔE_{elec}	ΔE_0	$\Delta H^{o/‡}$	$\Delta G^{o/‡}$
10[a]	−4.55	−3.60	−3.60	−2.15
11-TS[a]	18.47	19.73	19.73	19.66
12[a]	14.45	16.14	16.14	14.75
13-TS[a]	24.48	27.00	27.00	20.92
14[a,b]	24.85	26.49	27.09	14.36
15[b]	7.20	9.64	9.64	10.15
16-TS[b]	13.95	16.12	16.12	16.80
17[b]	12.20	14.69	14.69	14.48
18-TS[b]	13.96	16.04	16.04	18.00
19[b]	−6.21	−4.36	−4.36	−1.26

[a] + C$_6$H$_6$. [b] + CH$_4$ energies are reported in kcal·mol^{-1} and relative to **1**.

The molecular geometries for complexes **11**−**19** are analogous to the complexes involved in the first methane elimination and benzene addition events, and these representations are included in Supporting Information Figure 1. Calculated relative energies for complexes **1**−**19** are reported in Table 2. The calculated bond lengths of **19** are in agreement with the bond lengths found in the crystal structure, and this result is shown in Figure 7. The overall reaction is calculated to be exothermic and exergonic by 4.36 and 1.26 kcal·mol^{-1}, respectively. To compare the two methane release events, the analogues of Ba1 and Ba2, in this second replacement, are 1 and 3 kcal·mol^{-1} less than the B3LYP/BS1 values of Ba1 and Ba2 for the first replacement. The analogous barriers are defined as **11-TS** and **14**, and both are relative to **10**. As with the addition of the first benzene, the transition state for benzene addition to **14** was not located; however, ***TS*** is estimated and included in Figure 6.

2. Alternative Pathways. In this section, alternative pathways are explored for the C−H coupling and methane

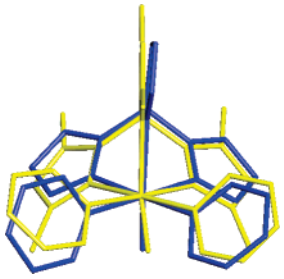

Figure 7. The crystal structure for κ^3-Tp*Pt^{IV}(Ph)$_2$H (yellow) and the B3LYP/BS1 equilibrium geometry for κ^3-TpPt^{IV}(Ph)$_2$H (blue) are overlaid. Bond lengths and angles are in general agreement between the two structures.

Table 3. Relative B3LYP/BS1 Energies (kcal·mol^{-1}) for *Rotation* and *Inversion* Mechanisms

	energies			
complex	ΔE_{elec}	ΔE_0	$\Delta H^{o/‡}$	$\Delta G^{o/‡}$
1[a]	0	0	0	0
TS$_{1-1a}$[a]	21.77	21.77	21.65	21.93
1a	21.28	21.28	21.60	20.92
2a-TS[a]	27.23	27.23	27.46	26.37
3a[a]	21.88	21.88	22.48	20.66
5a[a,b]	33.47	33.47	34.67	21.41
TS$_{1-1b}$[a]	32.16	32.16	32.06	31.27
1b[a]	22.82	22.82	23.32	21.78
2b-TS[a]	26.00	26.00	26.20	25.33
3b[a]	19.98	19.98	20.60	18.86
5b[a,b]	30.94	31.54	32.13	19.17

[a] + C_6H_6. [b] + CH_4 energies are reported in kcal·mol^{-1} and relative to **1**.

release. The possibility of an associative mechanism is examined where benzene coordinates prior to methane release. Two possible orientations of a pyrazolyl (pz) ring are also examined: (1) ring *rotation* about a B−N bond resulting in a side-on interaction of a pz ring with platinum and (2) *inversion* of the boron so that a pz ring is completely removed from the ligand sphere. Last, the possible formation of a dimer is examined. The relative energies are tabulated for the *rotation* and *inversion* pathways in Table 3, and these pathways are shown in Figure 8. In Figure 9, representative geometries are presented for complexes on the *rotation* and *inversion* pathways; and the difference is shown between the binding modes of the Tp ligand. The complexes along the *rotation* and *inversion* pathways not shown in Figure 9 are shown in Supporting Information Figure 2. All structures were calculated at the B3LYP/BS1 level of theory, as in section 1.

Though the experimental work by Jensen et al. supported a dissociative mechanism for methane loss, evidence for an associative mechanism for methane loss was reported by Johansson and Tilset where increased concentrations of solvent acetonitrile changed the ratio of CH_4/CH_3D released from protonated Pt^{II} complexes.[28] Therefore, several models were designed to investigate the possible associative mechanism where benzene and methane are both bound simultaneously to the platinum center; the benzene and methane are π- and σ-bound to the platinum center, respectively. All attempts to locate a transition state geometry for an associative complex were unsuccessful, and our data support the dissociative mechanism (Figure 2).

The next alternative pathway (*rotation*) is described by rotation of the pz ring *axial* to the hydride about the B−N$_{pz}$ bond (N$_{pz}$ is the nitrogen of the *axial* pz ring bonded to the boron) and formation of a complex where two pz rings are coordinated as usual and the third pz ring has "slipped" to form a κ^2-, κ'-Tp complex (**1a**). The barrier to pz ring rotation is 21.7 kcal·mol^{-1} (**TS$_{1-1a}$**). The N$_{pz}$ has a small amount of 4-coordinate character as the B−N$_{pz}$−Pt angle is 89.7° (Figure 9), and the Pt−N$_{pz}$ distance is 2.69 Å, which is ca. 0.5 Å longer than the Pt−N$_{ax}$ distance in **1**. The barrier to C−H coupling (**2a-TS**) is slightly greater than that of the

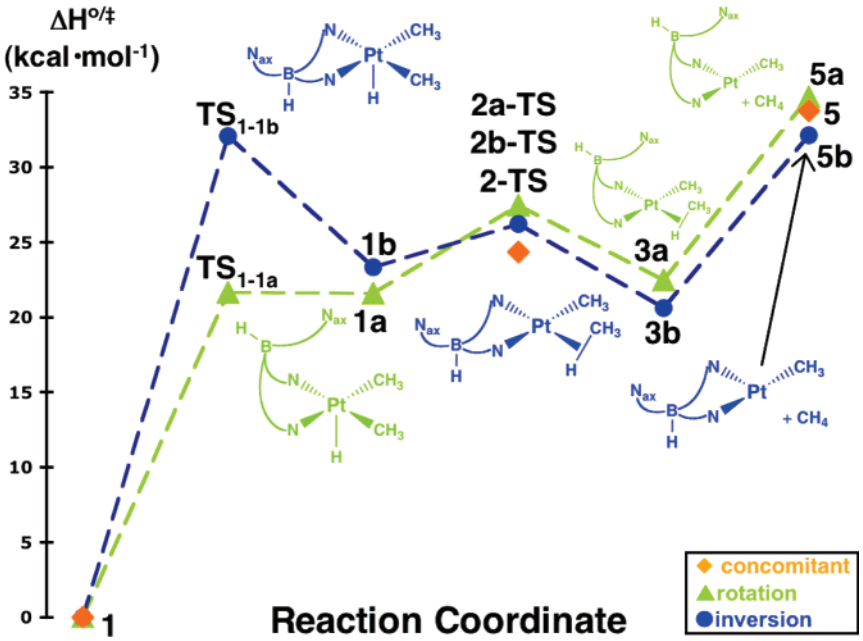

Figure 8. A comparison between the enthalpic PES for the concomitant (orange diamonds), *inversion* (blue dots), and *rotation* (green triangles) pathways leading to C−H bond formation (RE) and methane release. The energies, relative to **1**, are in kcal·mol^{-1}.

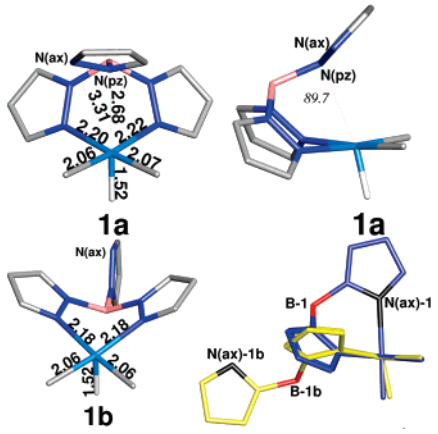

Figure 9. The B3LYP/BS1 optimized geometries for κ^2-, κ'-TpPt^{IV}(CH$_3$)$_2$H (**1a**) and κ^2-TpPt^{IV}(CH$_3$)$_2$H (**1b**) and the comparison between the starting material (**1**-blue) and the inverted form (**1b**-yellow). Bond lengths are reported in Å.

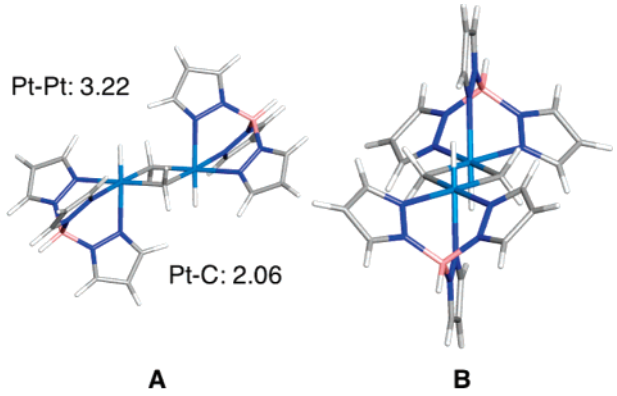

Figure 10. Two different views of the dimer complex. The view in **A** is down the bridging carbon−carbon atoms, while the view in **B** is down the Pt−Pt axis of the molecule. The opposing geometry of the Tp ligands is represented clearly in **A**.

concomitant pathway in Figure 1 (*rotation*: 27.5 vs *con*: 24.1 kcal·mol^{-1}), and a pseudo-square planar (4-coordinate) complex (**3a**) is the result of C−H coupling. As with the *concomitant* pathway, the 16e$^-$, coordinatively-unsaturated Pt^{II} (d^8) complex that results from methane loss (**5a**) is stabilized by an increase in the interaction of the pz ring that was trans to the hydride but is now trans to the vacant coordination site.

In the *inversion* pathway, the *axial* pz ring is removed from the ligand sphere by inversion of the boron geometry, which results in a κ^2-Tp ligand. The barrier to inversion (**TS$_{1-1b}$**) is 32.1 kcal·mol^{-1}, which is the highest initial barrier of any of these pathways. A 5-coordinate Pt^{IV} species (**1b**) is formed where the *axial* pz ring is outside of the coordination sphere, and the boron is shown to reside below the *equatorial* pz rings (Figure 9). The C−H bond coupling transition state (**2b-TS**) is 26.6 kcal·mol^{-1} (relative to **1**), which is slightly greater than the *concomitant* pathway. A weakly bound methane complex is formed (**3b**), and loss of methane from this complex results in a 3-coordinate, Pt^{II} complex. This pathway has the lowest value for Ba2 of the three pathways at 32.1 kcal·mol^{-1}.

Summary of the Two Alternative Pathways. Facile C−H activation of benzene by [κ^2-[Ph$_2$B(pz)$_2$]Pt^{II}(Me)$_2$]$^+$ was reported by Thomas and Peters;[29] however, the *inversion* pathway is disfavored because the initial barrier (**TS$_{1-1b}$**) is higher in energy. Both barriers along the *rotation* pathway are similar to those of the *concomitant* pathway. The calculated values for Ba1 and Ba2 are not significantly altered when the interaction between the *axial* pz ring and the platinum is changed (*rotation*) or removed (*inversion*). A difference of 10.4 kcal·mol^{-1} is measured between the initial barriers to the *inversion* and *rotation* pathways ($\Delta\Delta H$: **TS$_{1-1b}$** − **TS$_{1-1a}$**); this difference is slightly greater than the difference of 6.4 kcal·mol^{-1} that was reported by Webster and Hall for the same barriers in the isomerization chemistry of TpRh(CO)$_2$.[30]

In a mixture of TpRu(PMe$_3$)$_2$OH and 1-methylpyrazole in C$_6$D$_6$, H/D exchange was reported by Gunnoe and coworkers at the four position of each pz ring, and this mechanism likely proceeds through a pathway where the pz ring coordinates to the ruthenium in a side-on interaction.[31] This experimental observation supports a competitive route via the *rotation* pathway. The *rotation* and *concomitant* pathways compete in the elimination of methane because of these similar relative energies.

Possible Formation of a [TpPt]$_2$ Dimer. A dimer was not observed in the kinetic studies of C−H coupling and methane release, but other studies have reported the formation and isolation of bridged binuclear complexes.[32] A common structural characteristic of the binuclear structures observed experimentally is opposing ligand geometries as seen in the calculated structure, Figure 10. Species **5** has an open coordination site available for dimer formation with a second molecule of **5**. In the optimized geometry of the calculated dimer, the two TpPt moieties are joined by a 4-center, 8e$^-$ bridge. In addition to reformation of the Pt−H bond, the Tp ligand returns to a tridentate interaction with the platinum. Dimer formation from **1** (2·**1** → dimer + 2·CH$_4$) is exergonic (−4.5 kcal·mol^{-1}) and endothermic (2.4 kcal·mol^{-1}); because of its instability, the dimer was not studied further.

3. Bonding Analysis. To investigate the bonding interactions that are involved in this chemistry, the B3LYP/BS1 electron densities of complexes **1**, **2-TS**, **3**, **5**, and **1a** were investigated with Bader's "Atoms in Molecules" (AIM) analysis.[33] Specific bond critical point (CP) densities that are relevant to the C−H coupling and methane release chemistry are tabulated in Table 4. AIM2000 was used to calculate the bond CPs.[34]

The electron density of **1** was analyzed with AIM, and six (3, −1) bond CPs were found between the platinum and the atoms listed in Table 4. The Pt−N$_{ax}$ bond CP has the least density, which results from the stronger trans influence of the hydride. The bond CP densities typically follow an inverse trend with respect to bond lengths; for example, the Pt−N$_{eq}$(r) bond CP density increases with C−H coupling and methane release, and the bond length shortens for this process. The Pt−C$_{Me}$(r) and −N$_{eq}$(l) bond densities are shown to be insensitive to the C−H coupling chemistry, and this correlates with geometric observations. Interestingly, a Pt−C$_{Me}$(l) bond CP was not located in the density of **2-TS** and

Table 4. Bond Critical Point (CP) Densities for Bonds Involved in C−H Coupling and Methane Release

	(3, −1) bond CP density (ρ(r)/e·bohr^{-3})				
bond: Pt−X	**1**	**2-TS**	**3**	**5**	**1a**
N_{ax}	0.0727040408	0.0241899527	0.0139997372	0.0167954419	NA
N_{eq}(l)	0.0757628782	0.0791088190	0.0811165097	0.0825009156	0.0795292241
N_{eq}(r)	0.0756648650	0.0979133965	0.1203747575	0.1334978956	0.0765416921
C_{Me}(l)	0.1329266488	NF[b]	NF	NA	0.1348946156
C_{Me}(r)	0.1330781962	0.1329927831	0.1337466884	0.1403112418	0.1336717972
H	0.1741331362	0.1485854220	0.0831396505	NA	0.1816352613
N_{pz}	NA[a]	NA	NA	NA	0.0304053343

[a] NA = not applicable. [b] NF = not found.

3; thus, the bond is manifested solely by a CP between the platinum and the hydrogen. For **1a** (one pz rotated), a bond CP was located along the Pt−N_{pz} coordinate with a density of 0.030405 e·bohr^{-3}, which is significantly less than the Pt−N_{ax} bond CP density value of **1**. The decrease in bond CP density is consistent with an increase in bond lengths, but the multiple CPs that are characteristic of a ligand π-bound to a metal (i.e., η^5-C_5H_5) are not observed for this rotated pz ring.

4. Density Functional and Basis Set Benchmarking. Benchmarking studies of density functionals and basis sets are presented in this section. Thirty-one functionals were benchmarked for the barriers. Basis set saturation was also studied, and the trends are presented. The procedure that was used for these studies is explained prior to each benchmarking study. The mean average error (mae) is reported for each study.

Functionals. For all but two of the functionals, the optimized geometry and analytical frequencies of **1**, **2-TS**, **5**, and methane were calculated at the functional/BS1 level of theory. Intermediates and transitions states were verified as having zero and one imaginary mode, respectively, as determined by frequency calculations. To calculate the barrier value at each level of theory, the functional/BSX//functional/BS1 (X = 2, 3) energies of **1**, **2-TS**, **5**, and methane were added to the function/BS1 correction to the enthalpy for each complex. For BS2 and BS3 basis sets, only the cc-pVDZ basis set of BS1 was replaced with cc-pVTZ and cc-pVQZ in BS2 and BS3, respectively, but the other basis sets remained as assigned in BS1. *All subsequent calculated values for the two barriers are presented at the functional/BS3 level of theory*. The procedure for the B2-PLYP[35] and mPW2-PLYP[36] functionals was slightly modified because of computational costs; the B2-PLYP/BSX// and mPW2-PLYP/BSX//B3LYP/BS1 (X = 1, 2, 3) energies of **1**, **2-TS**, **3**, **5**, and methane were added to the second-order correction and the B3LYP/BS1 correction to the enthalpy for each molecule to obtain the corrected enthalpy. The second-order perturbative correction was scaled by 0.27 and 0.25 for the B2-PLYP and mPW2-PLYP functionals, respectively.[37]

Pure density functionals, in which exact exchange is not incorporated, included in this study are BLYP,[38,20b] BPW91,[38,39b] BP86,[38,40] G96LYP,[41,20b] G96PW91,[41,39b] HCTH,[42] mPWPW91,[39] and PBE.[43] Hybrid density functionals (HDFT), which include a percentage of Hartree−Fock (exact) exchange, included in this study are the B3LYP,[20] B3PW91,[20a,39b] B3P86,[20a,40] B97-1,[44] mPW1PW91 (mPW0),[39b] PBE1PBE (PBE0),[43] MPW1K,[45] BH&HLYP,[46,20b] and MPWLYP1M.[47] Two newly developed hybrid functionals that include contributions from unoccupied virtual orbitals via perturbation theory are included in this report: B2-PLYP and mPW2-PLYP. Meta functionals (MDFT), which include the orbital kinetic energy component, included in this study are BB95,[38,48] mPWB95,[39a,48] mPWKCIS,[39a,49] PBEKCIS,[43,49] TPSS,[50] and VSXC.[51] Hybrid meta functionals (HMDFT), which includes exact exchange into meta functionals, employed in this study are B1B95,[48] MPWKCIS1K,[52] BB1K,[53] MPWB1K,[54] MPW1B95,[54] and TPSSh.[55]

Barrier 1. The values of Ba1, calculated with all the functionals previously mentioned, are shown in Figure 11. A value for Ba1 within 5 kcal·mol^{-1} of experiment, which is the typical margin of error for DFT in calculating barrier heights, was calculated for all but three of the functionals tested. However, a value within 1 kcal·mol^{-1} of experiment, which is the definition for "chemical accuracy" of a calculation, was calculated with the BPW91, G96LYP, G96PW91, B3P86, B97-1, mPW0, MPW1K, BH&HLYP, BB1K, and MPWB1K functionals. The error in these calculations is systematically below the experimental value; only the TPSS, TPSSh, BB1K, B2-PLYP, and mPW2-PLYP functionals calculated a value greater than the experimental value. Generally, the accuracy of the calculation does increase when exact exchange is included in the functional; for example, the MPW1K, BB1K, and MPWB1K return values that are more accurate than the mPWPW91, BB95, and mPWB95 parent functionals. The average value and standard deviation were calculated for each DFT category, and these numbers are included in Figure 11. A particularly poor value for Ba1 was calculated with the VSXC functional because the VSXC/BS1 optimized geometry of **2-TS** is similar to the structure of **2a-TS** where the *axial* pz ring has rotated to form the side-on interaction. For Ba1, a value of 24.3 kcal·mol^{-1} was calculated by using the HF method (HF/BS3 level of theory) and following the same procedure for this calculation as was performed with the density functionals.

Barrier 2. In Figure 12, the calculated value of Ba2 is presented for each functional and for the average values for each functional group. A value for Ba2 within 5 kcal·mol^{-1} was calculated for all but four of the functionals tested; however, a value within chemical accuracy was calculated for only the BPW91, MPWLYP1M, B3LYP, mPWKCIS, and PBEKCIS functionals. The accuracy and precision in calculating Ba2 is poorer for each functional category; the

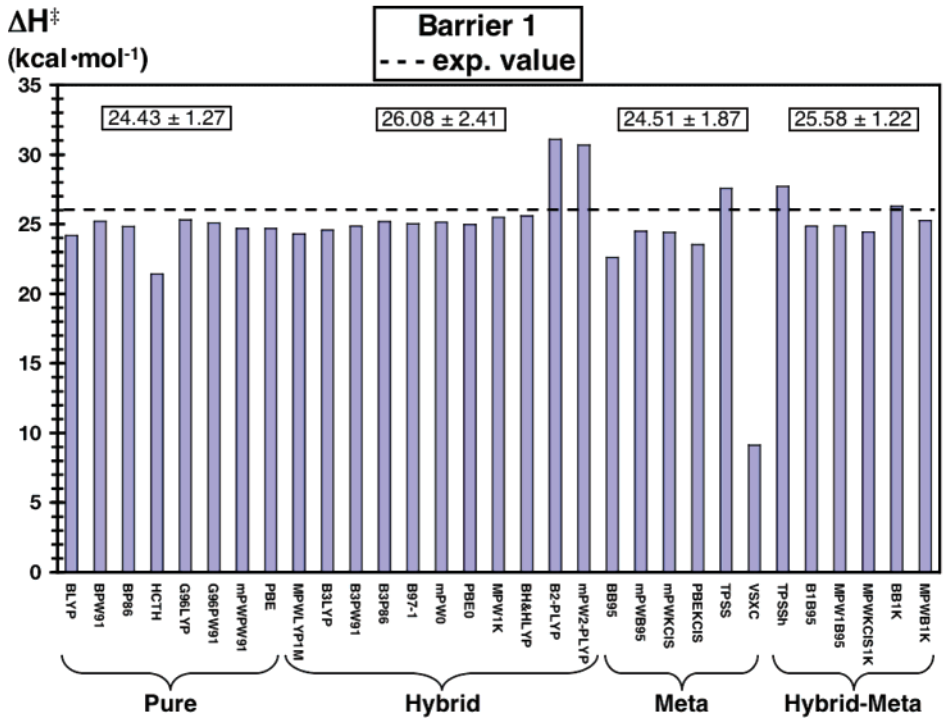

Figure 11. The calculated value for Ba1 for each functional. The dashed line represents the experimental value. In the boxes, the average values with standard deviations are presented for each group. The VSXC functional failed the Q-test (C.I. 90%) that was applied to the meta group and was not included in the statistics.

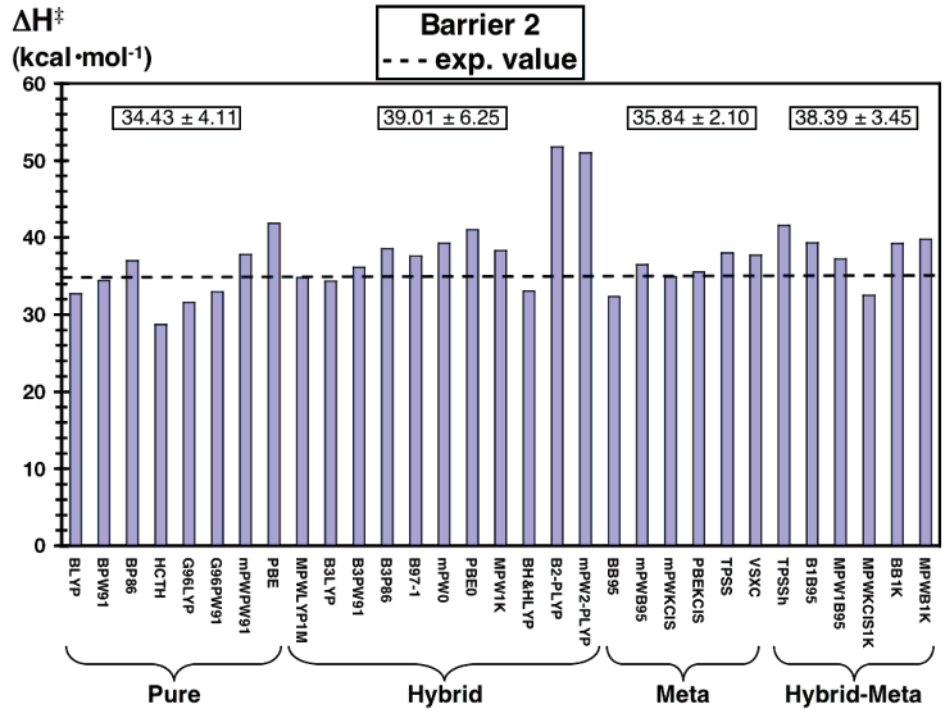

Figure 12. The calculated value of Ba2 for each functional. The dashed line represents the experimental value. The numbers in the boxes are the average values with standard deviations for each DFT category.

meta category is the most accurate and precise group. For Ba2, the calculated value does increase when exact exchange is included in the functional, but the accuracy generally decreases; for example, the meta group has a smaller average value and a lower deviation than the hybrid-meta group. At the HF/BS3 level of theory, a value of 11.2 kcal·mol^{-1} was calculated for Ba2.

Statistical Analysis. The mae for the functionals tested are listed in Table 5, and these values were determined for the results calculated at the functional/BS3 level of theory. From this error analysis, the best performing pure, hybrid, meta, and hybrid-meta density functionals are BPW91, MPWLYP1M, mPWKCIS, and MPW1B95, respectively; and the best overall performer is the BPW91 functional.

Table 5. mae for the Functionals Tested in This Report

pure		hybrid		meta		hybrid-meta	
functional	mae	functional	mae	functional	mae	functional	mae
BLYP	2.05	MPWLYP1M	*0.95*	BB95	3.04	TPSSh	4.15
BPW91	***0.68***	B3LYP	1.05	mPWB95	1.52	B1B95	2.74
BP86	1.58	B3PW91	1.15	mPWKCIS	*0.84*	MPW1B95	*1.68*
G96LYP	5.44	B3P86	2.18	PBEKCIS	1.51	MPWKCIS1K	2.03
G96PW91	1.48	B97−1	1.77	TPSS	2.28	BB1K	5.46
HCTH	2.04	mPW0	2.58	VSXC	9.81	MPWB1K	2.76
mPWPW91	2.06	PBE0	3.52				
PBE	4.07	MPW1K	1.93				
		BH&HLYP	1.17				
		B2-PLYP	10.92				
		mPW2-PLYP	10.33				

Summary of Density Functional Benchmarking Studies. Overall, the accuracy of the calculations is greater for Ba1 than for Ba2; the errors in the individual calculation of **5** and methane are summed, which decreases the accuracy of the calculations of Ba2. In previous studies, more accurate values for barriers were calculated with functionals where greater amounts of exact exchange were admixed into the functionals,[56] and this trend is supported with the data for Ba1. For example, the calculated value for Ba1 with the BLYP, B3LYP, and BH&HLYP functionals approaches the experimental value as the amount of exact exchange admixed into the functional increases. For both barriers, the average value increases when exact exchange is incorporated into the functionals; however, the deviation generally increases (Figures 11 and 12). In order to measure the effect of changing between common exchange and correlation functionals, the LYP, PW91, and P86 correlation functionals were paired with the B88 and B3 exchange functionals; and the general trend is that greater values (Ba1 and Ba2) were calculated in the order of LYP < PW91 < P86. The functionals with the B3 exchange functional calculated values that were greater than the corresponding functional with the B88 exchange functional. The only functional that calculated a value within 1 kcal·mol^{-1} for both barriers was BPW91. The B2-PLYP and mPW2-PLYP functionals, which include contributions from the virtual orbitals, are unsuitable for calculating these barrier heights as the values were much too high and diverged from experiment with basis set saturation.

Recently, Truhlar et al. performed a DFT benchmarking study[47] with a test set comprised predominantly of metal-containing compounds, and the G96LYP and MPWLYP1M functionals were shown to be suitable for these systems. In our study, more accurate values for Ba1 and Ba2 were returned with the MPWLYP1M functional. Quintal et al.[57] reported a benchmarking study of various functionals and found the kinetic functionals optimized for barrier heights (i.e., MPW1K) unsuitable for barriers of late row transition-metal reactions; in our study, these kinetic functionals performed well for Ba1 but not Ba2. The enthalpic values for Ba1 and Ba2 are tabulated for each functional in Supporting Information Table 1 at the BS1, BS2, and BS3 levels of theory.

Table 6. Results in Calculating Ba1 for Various ECP/BS That Were Assigned to Platinum[a]

no.	Pt: outermost 18e$^-$	ECP for Pt: inner 60e$^-$	$\Delta H^{\ddagger}$ Ba1 kcal·mol^{-1}
1	CRENBL	AREP	25.22
2	SBKJC	SBKJC	23.90
3	HW-VDZ (341/321/21)	LANL2	22.88
4	mLANL2DZ (341/341/21)	″	24.58
5	LANL2DZ(f) (341/341/21/1)	″	25.79
6	LANL2TZ (341/341/111)	″	24.95
7	SDD	Stuttgart RSC 1997	23.80
8	SDD(2f)	″	24.14
9	SV	″	21.80
10	TZVP	″	23.65
11	TZVPP	″	23.89
12	QZVP	″	20.38

[a] All other atoms were assigned the basis sets of BS3.

Basis Set Study. Only the first barrier (Ba1) was considered for the ECP/BS and all electron basis set benchmarking studies, and only the B3LYP functional was used in the large basis set study. Twelve ECP/BS were examined to measure the effect on the value of Ba1. The same procedure that was used to test the functionals was used here, but only the ECP/BS was replaced for each test. The geometries of **1** and **2-TS** were fully optimized with each ECP/BS (with the all-electron basis sets of BS1 for the first row elements), and single-point (SP) calculations were run on these optimized geometries with the ECP/BS and the all-electron basis sets of BS3 for the first row elements. These SCF energies were then added to the B3LYP/BS1 corrections to the enthalpy for **1** and **2-TS** to obtain the relative enthalpy difference. Four ECPs were used in this study for the inner 60e$^-$ of platinum, and they are the Hay and Wadt LANL2,[21] the Stuttgart relativistic small core (RSC) 1997[58] ECP, the averaged relativistic (AREP) ECP of Ross et al.,[59] and the relativistic compact effective potential (RCEP) of Stevens et al. (SBKJC).[60] The basis sets coupled with the ECPs are the Hay and Wadt valence double-ζ BS[61] (HW-VDZ); the mLANL2DZ BS of Couty and Hall as previously mentioned;[22] the valence double-ζ SBKJC BS of Steven et al.;[60] the Stuttgart/Dresden double-ζ SDD[58] BS; the split valence (SV), triple-ζ with one (TZVP) and two (TZVPP) polarization functions, and quadruple-ζ with one polarization function (QZVP) of Weigend and Ahlrichs.[62]

In Table 6, the results of benchmark studies are shown for the platinum ECP/BS considered in this study. For each

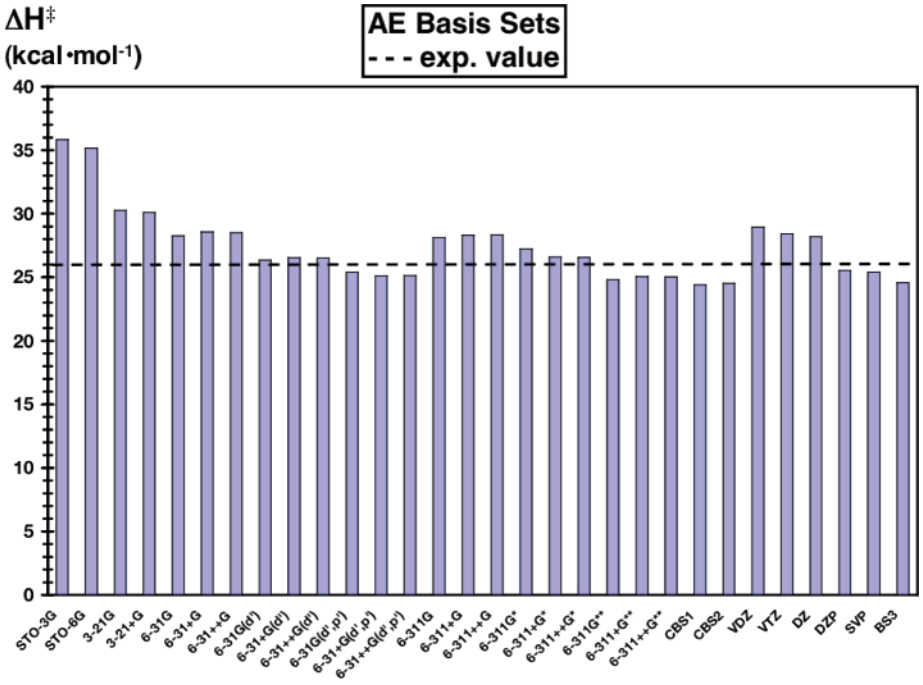

Figure 13. The effect of the basis set on the value of Ba1. The B3LYP/BS1 geometries were used in this study, and all non-platinum elements were assigned the basis set listed. The experimental value of Ba1 is represented by the dashed line.

BS used in this study, the addition of a polarization function resulted in an increased value calculated for Ba1. The modification of Couty and Hall to the HW-VDZ BS improved the value by nearly 2 kcal·mol^{-1}, while decontracting the d shell to form a triple-ζ quality BS returned a similar value to that of the mLANL2DZ. Similar values for Ba1 were calculated with the TZVP and TZVPP BS; however, the values that were calculated with the SV and QZVP BS are the lowest in this study. Of all the ECP/BS that were assigned to platinum, the SV and QZVP BS are the poorest for calculating the value of this barrier.

To benchmark the all-electron basis sets for the first row elements, platinum was assigned the ECP/BS of BS1, and the first row atoms were assigned the same basis sets from the list of Pople's n-Gaussian[63] (STO-nG, $n = 3,6$) basis sets; Pople-style split valence[64] from 3-21G to 6-311++G**; Dunning's full double-ζ basis set (DZ), double-ζ plus polarization basis set (DZP),[65] and split valence plus polarization (SVP) basis set;[66] and Ahlrich's valence double- and triple-ζ basis sets (VDZ, VTZ).[67] To measure basis set saturation, the large basis sets of the complete basis set atomic pair natural orbital (CBS-APNO) method of Petersson and co-workers were used,[68] and these basis sets are denoted CBS1 and CBS2.[69] To obtain the calculated value for Ba1, the SCF energies from these SP calculations were added to the B3LYP/BS1 correction to the enthalpy.

The results are shown in Figure 13 for the all-electron basis set benchmarking study. The most important factor for calculating accurate barrier values is the addition of polarization functions to the basis set, and this trend is seen for each family of basis sets. Diffuse functions, applied either to non-hydrogen atoms (+) or to all atoms (++), did not significantly alter the calculated value compared to the same basis sets without the diffuse functions. Increasing the size of the basis sets from double- to triple-ζ did not significantly alter the calculated value for the barrier. Basis set saturation was reached at the CBS1 level of theory as the addition of two f polarization functions to CBS1, producing CBS2, did not alter the calculated value of Ba1. The energies for each basis set is included in Supporting Information Table 2.

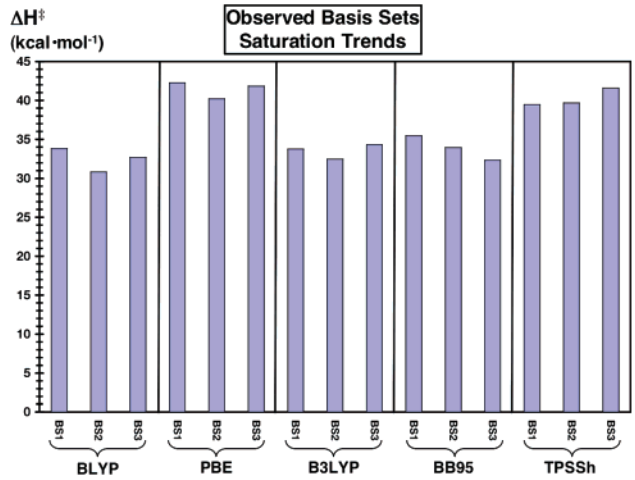

Figure 14. The three basis set saturation trends observed in this work. The trends represented by BLYP, PBE, and B3LYP are representative for most of the functionals tested. The exceptions are discussed in the text.

Basis Sets and Functionals. The trends in basis set saturation (BSS) are shown in Figure 14. For most of the functionals tested, the BSS trend is unexpected because the value calculated at the cc-pVTZ (BS2) level of theory is less than that of both the cc-pVDZ (BS1) and cc-pVQZ (BS3) levels of theory, and the data presented for the BLYP, PBE, and B3LYP functionals are representative for most of the functionals. However, there are exceptions; an expected BSS trend is observed for BB95 (Ba1 & Ba2) where the calculated value decreases with the increase in basis set size, while the

BSS trend for the TPSSh values increase and diverge from the experimental value (Ba2 only). The B2-PLYP and mPW2-PLYP functionals exhibit a similar trend as with TPSSh but for both barriers. For example, the values for Ba1 and Ba2, calculated with the B2-PLYP functional, increase from 27.7 to 31.1 and from 42.8 to 51.7 kcal·mol^{-1} for the BS1, BS2, and BS3 levels of theory, respectively.

Conclusion

We presented the reaction mechanism for the conversion of **1** into **19**, where the important mechanistic barriers to C−H coupling and methane release were analyzed. Against the experimental values of these barriers, 31 density functionals were benchmarked, and, within the definition of "chemical accuracy", 11 were found to be accurate for calculating the C−H coupling barrier, while only 5 were accurate for calculating the value of Ba2. In general, more accurate values for Ba1 were calculated with the functionals with higher values of exact exchange (ca. 40%) admixed into the functional, but those functionals did not perform well for calculating the dissociation barrier. Many of the common ECP/BS combinations available for platinum were found to be suitable for calculating reaction barriers; and polarization functions, added to each all electron basis set, were shown to be a requirement. In this study, DFT was shown to be a suitable method for including electron correlation, as it greatly outperformed the Hartree−Fock theory in calculating these two barriers.

Acknowledgment. This work was supported by grants from the NSF (CHE-0518074 and DMS-0216275) and The Welch Foundation (A0648). The authors thank Chad Beddie for valuable discussions.

Supporting Information Available: Every value for Ba1 and Ba2 (calculated with each functional and basis set), optimized geometries of complexes **11-TS**−**19**, and the remaining complexes for the *rotation* and *inversion* pathways. This material is available free of charge at http://pubs.acs.org.

References

(1) (a) Williams, T. J.; Labinger, J. A.; Bercaw, J. E. *Organometallics* **2007**, *26*, 281−287. (b) Zhang, F.; Kirby, C. W.; Hairsine, D. W.; Jennings, M. C.; Puddephatt, R. J. *J. Am. Chem. Soc.* **2005**, *127*, 14196−14197. (c) Heyduk, A. F.; Driver, T. G.; Labinger, J. A.; Bercaw, J. E. *J. Am. Chem. Soc.* **2004**, *126*, 15034−15035. (d) Owen, J. S.; Labinger, J. A.; Bercaw, J. E. *J. Am. Chem. Soc.* **2006**, *128*, 2005−2016. (e) Konze, W. V.; Scott, B. L.; Kubas, G. J. **2002**, *124*, 12550−12556. (f) *Activation and Functionalization of C−H Bonds*; Goldberg, K. I., Goldman, A. S., Eds.; Oxford University Press: Washington, DC, 2004; pp 1−440.

(2) Garnett, J. L.; Hodges, R. J. *J. Am. Chem. Soc.* **1967**, *89*, 4546−4547.

(3) (a) Gol'dshleger, N. F.; Tyabin, M. B.; Shilov, A. E.; Shteinman, A. A. *Russ. J. Phys. Chem.* **1969**, *43*, 1222−1223 (English translation). (b) Shilov, A. E.; Shul'pin, G. B. *Chem. Rev.* **1997**, *97*, 2879−2932. (c) Shilov, A. E. *Activation of Saturated Hydrocarbons by Transition Metal Complexes*; D. Riedel: Dordrecht, The Netherlands, 1984; pp 1−203. (d) Shilov, A. E.; Shul'pin, G. B. *Activation and Catalytic Reactions of Saturated Hydrocarbons in the Presence of Metal Complexes*; Kluwer: Dordrecht, The Netherlands, 2000; pp 1−534.

(4) (a) Stahl, S. S.; Labinger, J. A.; Bercaw, J. E. *Angew. Chem., Int. Ed.* **1998**, *37*, 2180−2192. (b) Lersch, M.; Tilset, M. *Chem. Rev.* **2005**, *105*, 2471−2526.

(5) Fekl, U.; Kaminsky, W.; Goldberg, K. I. *J. Am. Chem. Soc.* **2001**, *123*, 6423−6424.

(6) Fekl, U.; Goldberg, K. I. *J. Am. Chem. Soc.* **2002**, *124*, 6804−6805.

(7) Crumpton, D. M.; Goldberg, K. I. *J. Am. Chem. Soc.* **2000**, *122*, 962−963.

(8) Procelewska, J.; Zahl, A.; Liehr, G.; van Eldik, R.; Smythe, N. A.; Williams, B. S.; Goldberg, K. I. *Inorg. Chem.* **2005**, *44*, 7732−7742.

(9) Reinartz, S. R.; White, P. S.; Brookhart, M.; Templeton, J. L. *J. Am. Chem. Soc.* **2001**, *123*, 6425−6426.

(10) Reinartz, S. R.; White, P. S.; Brookhart, M.; Templeton, J. L. *J. Am. Chem. Soc.* **2001**, *123*, 12724−12725.

(11) Norris, C. M.; Templeton, J. L. *Organometallics* **2004**, *23*, 3101−3104.

(12) Siegbahn, P. E. M.; Crabtree, R. H. *J. Am. Chem. Soc.* **1996**, *118*, 4442−4450.

(13) (a) Bartlett, K. L.; Goldberg, K. I.; Borden, W. T. *J. Am. Chem. Soc.* **2000**, *122*, 1456−1465. (b) Barlett, K. L.; Goldberg, K. I.; Borden, W. T. *Organometallics* **2001**, *20*, 2669−2678.

(14) Jensen, M. P.; Wick, D. D.; Reinartz, S.; White, P. S.; Templeton, J. L.; Goldberg, K. I. *J. Am. Chem. Soc.* **2003**, *125*, 8614−8624.

(15) Trofimenko, S. *Chem. Rev.* **1993**, *93*, 943−980.

(16) Wik, B. J.; Ivanovic-Burmazovic, I.; Tilset, M.; van Eldik, R. *Inorg. Chem.* **2006**, *45*, 3613−3621.

(17) Zarić, S.; Hall, M. B. *J. Phys. Chem. A* **1998**, *102*, 1963−1964.

(18) Parr, R. G.; Yang, W. In *Density Functional Theory of Atoms and Molecules*; Oxford University Press: New York, 1989; pp 1−333.

(19) Frisch, M. J.; Trucks, G. W.; Schlegel, H. B.; Scuseria, G. E.; Robb, M. A.; Cheeseman, J. R.; Montgomery, J. A., Jr.; Vreven, T.; Kudin, K. N.; Burant, J. C.; Millam, J. M.; Iyengar, S. S.; Tomasi, J.; Barone, V.; Mennucci, B.; Cossi, M.; Scalmani, G.; Rega, N.; Petersson, G. A.; Nakatsuji, H.; Hada, M.; Ehara, M.; Toyota, K.; Fukuda, R.; Hasegawa, J.; Ishida, M.; Nakajima, T.; Honda, Y.; Kitao, O.; Nakai, H.; Klene, M.; Li, X.; Knox, J. E.; Hratchian, H. P.; Cross, J. B.; Bakken, V.; Adamo, C.; Jaramillo, J.; Gomperts, R.; Stratmann, R. E.; Yazyev, O.; Austin, A. J.; Cammi, R.; Pomelli, C.; Ochterski, J. W.; Ayala, P. Y.; Morokuma, K.; Voth, G. A.; Salvador, P.; Dannenberg, J. J.; Zakrzewski, V. G.; Dapprich, S.; Daniels, A. D.; Strain, M. C.; Farkas, O.; Malick, D. K.; Rabuck, A. D.; Raghavachari, K.; Foresman, J. B.; Ortiz, J. V.; Cui, Q.; Baboul, A. G.; Clifford, S.; Cioslowski, J.; Stefanov, B. B.; Liu, G.; Liashenko, A.; Piskorz, P.; Komaromi, I.; Martin, R. L.; Fox, D. J.; Keith, T.; Al-Laham, M. A.; Peng, C. Y.; Nanayakkara, A.; Challacombe, M.; Gill, P. M. W.; Johnson, B.; Chen, W.; Wong, M. W.; Gonzalez, C.; Pople, J. A. *Gaussian 03, Revision C.02*; Gaussian, Inc.: Wallingford, CT, 2004.

(20) (a) Becke, A. D. *J. Chem. Phys.* **1993**, *98*, 5648−5652. (b) Lee, C.; Yang, W.; Parr, R. G. *Phys. Rev. B: Condens. Matter Mater. Phys.* **1988**, *37*, 785−789.

(21) Hay, P. J.; Wadt, W. R. *J. Chem. Phys.* **1985**, *82*, 270−283.

(22) Couty, M.; Hall, M. B. *J. Comput. Chem.* **1996**, *17*, 1359−1370.

(23) Dunning, T. H. *J. Chem. Phys.* **1989**, *90*, 1007−1023.

(24) Dunning, T. H.; Hay, P. J. *Modern Theoretical Chemistry*; Schaefer, H. F., III, Ed.; Plenum: New York, 1976; pp 1−28.

(25) (a) Manson, J.; Webster, C. E.; Pérez, L. M.; Hall, M. B. *JIMP 2 Version 0.091 (built for Windows PC)*; Department of Chemistry, Texas A&M University: College Station, TX, 2006 (available @ http://www.chem.tamu.edu/jimp2/index.html). (b) Hall, M. B.; Fenske, R. F. *Inorg. Chem.* **1972**, *11*, 768−779.

(26) (a) Hall, M. B.; Fan, H. *Adv. Inorg. Chem.* **2003**, *54*, 321−349. (b) Hartwig, J. F.; Cook, K. S.; Hapke, M.; Incarvito, C. D.; Fan, Y.; Webster, C. E.; Hall, M. B. *J. Am. Chem. Soc.* **2005**, *127*, 2538−2552.

(27) Johansson, L.; Tilset, M.; Labinger, J. A.; Bercaw, J. E. *J. Am. Chem. Soc.* **2000**, *122*, 10846−10855.

(28) Johansson, L; Tilset, M. *J. Am. Chem. Soc.* **2001**, *123*, 739−740.

(29) Thomas, C. M.; Peters, J. C. *Organometallics* **2005**, *24*, 5858−5867.

(30) (a) Webster, C. E.; Hall, M. B. *Inorg. Chim. Acta* **2002**, *330*, 268−282. (b) Webster, C. E.; Hall, M. B. *Inorg. Chim. Acta* **2002**, *336*, 168.

(31) Feng, Y.; Lail, M.; Foley, N. A.; Gunnoe, T. B.; Barakat, K. A.; Cundari, T. R.; Petersen, J. L. *J. Am. Chem. Soc.* **2006**, *128*, 7982−7994.

(32) (a) Reinartz, S.; Baik, M. H.; White, P. S.; Brookhart, M.; Templeton, J. L. *Inorg. Chem.* **2001**, *40*, 4726−4732. (b) Davies, M. S.; Hambley, T. W. *Inorg. Chem.* **1998**, *37*, 5408−5409. (c) Schwartz, D. J.; Andersen, R. A. *J. Am. Chem. Soc.* **1995**, *117*, 4014−4025.

(33) Bader, R. F. W. *Atoms in Molecules, A Quantum Theory*; Oxford University Press: Ithaca, NY, 1990; pp 1−438.

(34) AIM2000 designed by Friedrich Biegler-König, University of Applied Sciences: Bielefeld, Germany. https://www.aim2000.de/ (accessed month year).

(35) Grimme, S. *J. Chem. Phys.* **2006**, *124*, 034108.

(36) Schwabe, T.; Grimme, S. *Phys. Chem. Chem. Phys.* **2006**, *8*, 4398−4401.

(37) The values by which to scale the second-order correction were obtained by communication with the authors of refs 35 and 36.

(38) Becke, A. D. *Phys. Rev. A* **1988**, *38*, 3098.

(39) (a) Adamo, C.; Barone, V. *J. Chem. Phys.* **1998**, *108*, 664−675. (b) Perdew, J. P. In *Electronic Structure of Solids '91*; Ziesche, P., Eschig, H., Eds.; Akademie Verlag: Berlin, 1991; p 11.

(40) Perdew, J. P. *Phys. Rev. B* **1986**, *33*, 8822−8824.

(41) Gill, P. M. W. *Mol. Phys.* **1996**, *89*, 433−445.

(42) Hamprecht, F. A.; Cohen, A. J.; Tozer, D. J.; Handy, N. C. *J. Chem. Phys.* **1998**, *109*, 6264−6271.

(43) (a) Perdew, J. P.; Burke, K.; Ernzerhof, M. *Phys. Rev. Lett.* **1996**, *77*, 3865−3868. (b) Perdew, J. P.; Burke, K.; Ernzerhof, M. *Phys. Rev. Lett.* **1997**, *78*, 1396.

(44) Hamprecht, F. A.; Cohen, A. J.; Tozer, D. J.; Handy, N. C. *J. Chem. Phys.* **1998**, *109*, 6264−6271.

(45) Lynch, B. J.; Fast, P. L.; Harris, M.; Truhlar, D. G. *J. Chem. Phys. A* **2000**, *104*, 4811−4815.

(46) Becke, A. D. *J. Chem. Phys.* **1993**, *98*, 1372−1377.

(47) Schultz, N. E.; Zhao, Y.; Truhlar, D. G. *J. Phys. Chem. A* **2005**, *109*, 11127−11143.

(48) Becke, A. D. *J. Chem. Phys.* **1996**, *104*, 1040−1046.

(49) Krieger, J. B.; Chen, J.; Iafrate, G. J.; Savin, A. In *Electron Correlations and Materials Properties*; Gonis, A., Kioussis, N., Eds.; Plenum: New York, 1999; p 463.

(50) Tao, J.; Perdew, J. P.; Staroverov, V. N.; Scuseria, G. E. *Phys. Rev. Lett.* **2003**, *91*, 146401.

(51) Van Voorhis, T.; Scuseria, G. E. *J. Chem. Phys.* **1998**, *109*, 400−410.

(52) Zhao, Y.; González-Garcia, N.; Truhlar, D. G. *J. Phys. Chem. A* **2005**, *109*, 2012−2018.

(53) Zhao, Y.; Lynch, B. J.; Truhlar, D. G. *J. Phys. Chem. A* **2004**, *108*, 2715−2719.

(54) Zhao, Y.; Truhlar, D. G. *J. Phys. Chem. A* **2004**, *108*, 6908−6918.

(55) Tao, J.; Perdew, J. P. *J. Chem. Phys.* **2005**, *122*, 114102.

(56) (a) Truong, T. N.; Duncan, W. *J. Phys. Chem.* **1994**, *101*, 7408−7414. (b) Durant, J. L. *Chem. Phys. Lett.* **1996**, *256*, 595−602. (c) Boese, A. D.; Martin, J. M. L. *J. Chem. Phys.* **2004**, *121*, 3405−3416. (d) Mori-Sáchez, P.; Cohen, A. J.; Yang, W. *J. Chem. Phys.* **2006**, *125*, 201102. (e) Vydrov, O. A.; Scuseria, G. E. *J. Chem. Phys.* **2006**, *125*, 234109.

(57) Quintal, M. M.; Karton, A.; Iron, M. A.; Boese, A. D.; Martin, J. M. L. *J. Phys. Chem. A* **2006**, *110*, 709−716.

(58) Andrae, D.; Haussermann, U.; Dolg, M.; Stoll, H.; Preuss, H. *Theor. Chim. Acta* **1990**, *77*, 123−141.

(59) Ross, R. B.; Powers, J. M.; Atashroo, T.; Ermler, W. C.; LaJohn, L. A.; Christiansen, P. A. *J. Chem. Phys.* **1990**, *93*, 6654−6670.

(60) Stevens, W. J.; Krauss, M.; Basch, H.; Jasien, P. G. *Can. J. Chem.* **1992**, *70*, 612−630.

(61) Hay, P. J.; Wadt, W. R. *J. Chem. Phys.* **1985**, *82*, 299−310.

(62) Weigend, F.; Ahlrichs, R. *Phys. Chem. Chem. Phys.* **2005**, *7*, 3297−3305.

(63) (a) Hehre, W. J.; Stewart, R. F.; Pople, J. A. *J. Chem. Phys.* **1969**, *51*, 2657−2664. (b) Collins, J. B.; Schleyer, P. v. R.; Binkley, J. S.; Pople, J. A. *J. Chem. Phys*. **1976**, *64*, 5142−5151.

(64) 3-21G: Binkley, J. S.; Pople, J. A.; Hehre, W. J. *J. Am. Chem. Soc.* **1980**, *102*, 939−947. 6−31G: Hehre, W. J.; Pople, J. A. *J. Chem. Phys.* **1972**, *56*, 2257−2261. 6-311G: Krishnan, R.; Binkley, J. S.; Seeger, R.; Pople, J. A. *J. Chem. Phys.* **1980**, *72*, 650−654. Diffuse functions (+ & ++): Clark, T.; Chandrasekhar, J.; Sptiznagel, G. W.; Schelyer, P. v. R. *J. Comput. Chem.* **1983**, *4*, 294−301. Polarization functions: Foresman, J. B.; Frisch, *Æ*. *Exploring Chemistry with Electronic Structure Methods*, 2nd ed.; Gaussian, Inc.:

Pittsburgh, PA, 1996; p 110. The 6-31G(d′) basis set has the d polarization functions for C, N, O, and F taken from the 6-311G basis set instead of the original arbitrarily assigned value of 0.8 used in the 6-31G(d) basis set.

(65) Dunning, T. H. *J. Chem. Phys.* **1970**, *53*, 2823−2833.

(66) Dunning, T. H.; Hay, P. J. In *Methods of Electronic Structure Theory*; Schaefer, H. F., III, Ed.; Plenum Press: 1977; Vol. 2, pp 1−462.

(67) Schafer, A.; Horn, H.; Ahlrich, R. *J. Chem. Phys.* **1992**, *97*, 2571−2577.

(68) (a) Petersson, G. A.; Al-Laham, M. A. *J. Chem. Phys.* **1991**, *94*, 6081−6090. (b) Petersson, G. A.; Bennett, A.; Tensfeldt, T. G.; Al-Laham, M. A.; Shirley, W. A.; Mantzaris, J. *J. Chem. Phys.* **1988**, *89*, 2193−2218. (c) Montgomery, J. A., Jr.; Ochterski, J. W.; Petersson, G. A. *J. Chem. Phys.* **1994**, *101*, 5900−5909.

(69) Note, in Gaussian03 C.02, the keyword used to retrieve the APNO basis sets appears similar to the keywords for Pople double- and triple-zeta basis sets; however, APNO basis sets are not Pople basis sets. The 6-311G(d′,p′) keyword, defined in this current article as CBS1, calls for a (14s9p4d,6s3p1d)/[6s6p3d,4s2p1d] APNO basis set. The 6-311G(d′) keyword, defined in this current article as CBS2, calls for an APNO basis set that adds two f polarization functions to first row elements, (14s9p4d2f,6s3p1d)/[6s6p3d2f,4s2p1d].

CT700120D